Published in "International Journal of Quantum Chemistry 104(5):
695 - 715, 2005" which should be cited to reference this work.

Is the Vibrational Optical Activity of (R)-[$^2H_1$, $^2H_2$, $^2H_3$]-Neopentane Measurable?

WERNER HUG, JACQUES HAESLER

Department of Chemistry, University of Fribourg, Ch. du Musée 9, CH-1700 Fribourg, Switzerland

Received 17 November 2004; accepted 14 February 2005
Published online 11 April 2005 in Wiley InterScience (www.interscience.wiley.com).
DOI 10.1002/qua.20600

ABSTRACT: The compound, (R)-[$^2H_1$, $^2H_2$, $^2H_3$]-neopentane, with its T_d symmetric electron distribution, is the archetype of molecules that owe their chirality exclusively to an asymmetric distribution of the masses of their nuclei. It has nine rotamers, which fall into two classes, one where the interchange of hydrogen and deuterium nuclei leads to an identical rotamer, and one where it interconverts different rotamers. Ab initio computations show that individual rotamers have Raman optical activity (ROA) and vibrational circular dichroism (VCD) of the same size as ordinary chiral molecules. Dilution and cancelation for the experimentally accessible equilibrium mixture reduces ROA and VCD, but the simulation of spectra with realistic band shapes of the Voigt type shows that both remain measurable in the 700–1,400-cm^{-1} range, where ROA and VCD have a close to mirror image appearance. In the CH- and CD-stretch region, in contrast, the sign pattern of ROA and VCD is identical. This curious behavior appears to be a consequence of the differing influence of inertial contributions in the two spectral regions. If summed over all vibrations, ROA and VCD cancel neatly, as one expects from the T_d symmetric electron distribution.

Key words: vibrational optical activity; neopentane; Voigt line shape; inertial contributions

Introduction

Vibrational optical activity (VOA) depends on the chirality of a molecule's electron distribution as well as the chirality of the mass distribution of its nuclei. Measurements [1, 2] and theoretical considerations [3] have shown that the dissymmetry of nuclear motion is generally more important for generating VOA than the dissymmetry of the electron distribution, with the exception of resonance ROA [4]. A convincing demonstration of this fact is the observation that electronically achiral molecules, rendered chiral by isotope substitution only, can show VOA of the same size as the VOA one measures and calculates for molecules with an overall chiral structure.

Correspondence to: W. Hug; e-mail: w.hug@gmx.net
Contract grant sponsor: Swiss National Science Foundation.
Contract grant numbers: 2000-066679; 200020-103750.

Carbon atoms, substituted fourfold with physically distinguishable groups, have historically been considered the prime source of molecular chirality. Compounds derived from methane with three or four of its hydrogen atoms replaced by differing groups have often been discussed as chiral model compounds, and sometimes synthesized for studying their chiroptical properties [5]. With electronic optical activity, until recently the only physical method available for distinguishing enantiomers by spectroscopic means, one of the objectives of such work has been to test the limit to which similar, but not identical, substituents lead to measurable electronic optical rotatory dispersion or circular dichroism (CD) [6]. It does not appear, however, that [$^2H_1$, $^2H_2$, $^2H_3$]-neopentane has ever been discussed in such a context. One of the reasons may have been that its two enantiomers were judged a priori as not physically or chemically distinguishable.

With the advent of vibrational optical activity, ROA and VCD now exist as new spectroscopic techniques that should potentially be able to distinguish the R and S form of [$^2H_1$, $^2H_2$, $^2H_3$]-neopentane. Assessing the measurability of the ROA and VCD spectrum of this molecule has therefore been one of the reasons we have undertaken a theoretical study of its VOA. There are other aspects, however, which make the study of this interesting molecule worthwhile. It certainly represents the lightest stable molecule whose chirality can be traced to an asymmetrically substituted carbon atom and, in the absence of four stable isotopic species of hydrogen, fluorine, chlorine, and bromine, it is also the only gaseous or liquid compound in which the asymmetry of a carbon atom is due exclusively to the differing masses of its four substituents.

From the point of view of vibrational spectroscopy, comparison of the vibrations of [$^2H_1$, $^2H_2$, $^2H_3$]-neopentane with those of the nondeuterated and the fully deuterated form of the molecule is of interest. One can hope to gain a better understanding of the vibrational spectrum of the nonsymmetric molecule by relating it to those of the two symmetric ones. Understanding of how VOA is generated in small molecules, and in particular the knowledge of what structural elements lead to vibrational motion, producing large or negligible vibrational optical activity, is still quite limited. Analysis of the computed VOA of the title compound, which has a comparatively simple and fully symmetric electronic structure, can be expected to yield new insights into this important aspect of VOA.

Theoretical Expressions

VOA of molecular origin is measured for samples of randomly oriented molecules (an exception is the measurement of mulls in VCD, where the samples consist of randomly oriented crystallites embedded in a viscous solvent). Theoretical expressions for circular difference scattering (ROA) [7] and circular difference absorption (VCD) [8] therefore represent rotational averages over all orientations of a molecule. The situation for ROA is complicated by the fact that one has the option to measure it with different polarization schemes, by using different scattering geometries, and in resonance with electronic transitions. The formulae given below refer to the off-resonance situation, and the Placzek polarizability theory [9] is expected to apply for a molecule like [$^2H_1$, $^2H_2$, $^2H_3$]-neopentane. With respect to scattering geometries, only forward [10] and backward [1, 11] scattering have been considered, as little additional insight can be expected from either polarized or depolarized right-angle scattering. Numerical results are only reported for backward scattering, as the size of forward scattering turned out to be far too small to be measured.

For ROA, rotational averaging of the scattering tensor leads to combinations of tensor products that were first derived by Barron and Buckingham [12], and later shown by Long [13] to be expressible as linear combinations of invariants resulting from the double contraction of second-rank tensors. For VCD, the analogous quantity is the well-known rotational strength, the contraction of the magnetic and electric transition moment. A complication arises in VCD through the need to go beyond the Born–Oppenheimer approximation, by considering nuclear velocity as well, rather than nuclear excursion exclusively [14].

As has been shown explicitly elsewhere [15], all molecular Raman and ROA invariants can be conveniently expressed as the sum of terms that represent the contraction of a pair of nuclear displacement vectors with a diatomic electronic second-rank tensor. The same holds true for the electric dipole strength relevant for infrared (IR) absorption, and the rotational strength, which is relevant for VCD. The formulae for VCD can be obtained in a precisely analogous way as described for ROA, except that nuclear displacement has to be substituted by nuclear velocity for magnetic moments [16].

The differential Raman scattering cross section for forward or backward scattering into an infinitesimally small element of the solid angle is given by Ref. [13]:

$$d\sigma_p(0,\ \pi) = K_p\langle m_p|Q_p|n_p\rangle^2[90a_p^2 + 14\beta_p^2]d\Omega, \quad (1)$$

where n_p and m_p are the vibrational quantum numbers of the initial and final state, respectively, for vibration p. For Raman optical activity, the differential scattering cross section for forward scattering differs from that for backward scattering [3]:

$$-\Delta d\sigma_p(0) = \frac{4K_p}{c}\langle m_p|Q_p|n_p\rangle^2[90a_pG_p' + 2\beta^2_{Gp} - 2\beta^2_{\mathcal{A}p}]d\Omega \quad (2)$$

$$-\Delta d\sigma_p(\pi) = \frac{4K_p}{c}\langle m_p|Q_p|n_p\rangle^2[12\beta^2_{Gp} + 4\beta^2_{\mathcal{A}p}]d\Omega, \quad (3)$$

where Ω is the solid angle, and K_p is a constant that depends on the frequency ω_0 of the exciting light and the frequency ω_p of the scattered light, where p is the vibrational mode for which a transition between different states occurs:

$$K_p = \frac{1}{90}\left(\frac{\mu_0}{4\pi}\right)^2\omega_p^3\omega_0. \quad (4)$$

A minus sign has been included for difference expressions (2) and (3) because the sign convention in ROA for presenting data is opposite to that used in optical activity in general [17]. $-\Delta d\sigma$ corresponds to the ROA convention to represent the data measured or calculated for right circular light minus the data for left circular light, with $\Delta d\sigma$ defined in agreement with the standard convention left minus right used for molecular quantities in optical activity.

a^2 and β^2, without the index p, signify the isotropic and anisotropic invariant, respectively, of the molecular electric dipole–electric dipole polarizability tensor $\boldsymbol{\alpha}$, aG', and β^2_G the corresponding invariants of the cross product of this tensor with the electric dipole–magnetic dipole polarizability tensor $\mathbf{G}'$, and $\beta^2_{\mathcal{A}}$ the anisotropic invariant of it with the tensor $\mathcal{A}$ obtained by contracting the electric dipole–electric quadrupole tensor with the antisymmetric unit tensor of Levi–Cività. For a vibration p, the reduced invariants J_p, which do not include integration over vibrational wave functions, can be written in the general form

$$J_p = \sum_{\alpha,\beta}\mathbf{L}^x_{\alpha,p}\cdot\mathbf{V}_{\alpha\beta}\cdot\mathbf{L}^x_{\beta,p}. \quad (5)$$

They are related to the Raman and ROA invariants I, which in general are used for convenience without the index p of the vibration to which they pertain, as

$$I(1\ \leftarrow\ 0) = \langle 1|Q_p|0\rangle^2 J_p = \frac{\hbar}{2\Delta\omega_p}J_p. \quad (6)$$

In Eq. (6), the value of the integral over wave functions for a fundamental transition has been inserted

$$\langle 1|Q_p|0\rangle = \left(\frac{\hbar}{2\Delta\omega_p}\right)^{1/2}, \quad (7)$$

with Q_p the vibrational coordinate.

$\mathbf{L}^x_{\alpha,p}$, the Cartesian displacement vector of nucleus α with mass m_α in normal mode p, is normalized so that

$$\sum_{\alpha,i} m_\alpha(L^x_{\alpha i,p})^2 = 1. \quad (8)$$

The elements of the electronic second-rank tensors, or dyadics, $\mathbf{V}_{\alpha\beta}$, have the form:

$$V(a^2)_{ai,\beta j} = \frac{1}{9}\sum_{\mu,\nu}\left(\frac{\partial\alpha^e_{\mu\mu}}{\partial x_i^\alpha}\right)_0\left(\frac{\partial\alpha^e_{\nu\nu}}{\partial x_j^\beta}\right)_0 \quad (9a)$$

$$V(\beta^2)_{ai,\beta j} = \frac{1}{2}\sum_{\mu,\nu}\left[3\left(\frac{\partial\alpha^e_{\mu\nu}}{\partial x_i^\alpha}\right)_0\left(\frac{\partial\alpha^e_{\mu\nu}}{\partial x_j^\beta}\right)_0 - \left(\frac{\partial\alpha^e_{\mu\mu}}{\partial x_i^\alpha}\right)_0\left(\frac{\partial\alpha^e_{\nu\nu}}{\partial x_j^\beta}\right)_0\right] \quad (9b)$$

$$V(aG')_{ai,\beta j} = \frac{1}{9}\sum_{\mu,\nu}\left(\frac{\partial\alpha^e_{\mu\mu}}{\partial x_i^\alpha}\right)_0\left(\frac{\partial G'^{\,e}_{\nu\nu}}{\partial x_j^\beta}\right)_0 \quad (9c)$$

$$V(\beta^2_G)_{ai,\beta j} = \frac{1}{2}\sum_{\mu,\nu}\left[3\left(\frac{\partial\alpha^e_{\mu\nu}}{\partial x_i^\alpha}\right)_0\left(\frac{\partial G'^{\,e}_{\mu\nu}}{\partial x_j^\beta}\right)_0 - \left(\frac{\partial\alpha^e_{\mu\mu}}{\partial x_i^\alpha}\right)_0\left(\frac{\partial G'^{\,e}_{\nu\nu}}{\partial x_j^\beta}\right)_0\right] \quad (9d)$$

$$V(\beta^2_{\mathcal{A}})_{\alpha i,\beta j} = \frac{\omega_0}{2} \sum_{\mu,\nu} \left(\frac{\partial \alpha^e_{\mu\nu}}{\partial x^\alpha_i}\right)_0 \left(\frac{\partial \mathcal{A}^e_{\mu\nu}}{\partial x^\beta_j}\right)_0. \quad (9e)$$

Indices i and j refer to the Cartesian coordinates of nuclei α and β, and indices μ and ν to the Cartesian coordinate system in which the molecular tensors are defined.

The molar decadic extinction coefficient for vibrational absorption, and the difference of the extinction coefficients for left and right circular light, are given by [18]

$$\varepsilon_p(\tilde{\nu}) = \frac{20\pi^2 N_A}{3\varepsilon_0 hc \ln(10)} \tilde{\nu} \langle m_p|Q_p|n_p\rangle^2 D_p f(\tilde{\nu}_p, \tilde{\nu}) \quad (10)$$

$$\Delta\varepsilon_p(\tilde{\nu}) = \frac{80\pi^2 N_A}{3\varepsilon_0 hc^2 \ln(10)} \tilde{\nu}\, \mathrm{Im}\{\langle n_p|Q_p|m_p\rangle \times \langle m_p|\hat{P}_p|n_p\rangle\} R_p f(\tilde{\nu}_p, \tilde{\nu}), \quad (11)$$

where N_A is Avogadro's number, and $\tilde{\nu}_p$ the vibrational frequency in cm^{-1}.

The expressions for the reduced dipole strength D_p and the reduced rotational strength R_p are

$$D_p = \sum_{\alpha,\beta} \mathbf{L}^x_{\alpha,p} \cdot \mathbf{V}(D)_{\alpha\beta} \cdot \mathbf{L}^x_{\beta,p} \quad (12)$$

$$R_p = \sum_{\alpha,\beta} \mathbf{L}^x_{\alpha,p} \cdot \mathbf{V}(R)_{\alpha\beta} \cdot \mathbf{L}^x_{\beta,p}. \quad (13)$$

They are related to the ordinary dipole strength D and rotational strength R as

$$D(1 \leftarrow 0) = \langle 1|Q_p|0\rangle^2 D_p = \frac{\hbar}{2\Delta\omega_p} D_p \quad (14)$$

$$R(1 \leftarrow 0) = \mathrm{Im}\{\langle 0|Q_p|1\rangle\langle 1|\hat{P}_p|0\rangle\} R_p = \frac{\hbar}{2} R_p, \quad (15)$$

where in R the integral of the moment operator $\hat{P}$ for a fundamental transition has been used:

$$\langle 1|\hat{P}_p|0\rangle = i\left(\frac{\hbar\Delta\omega_p}{2}\right)^{1/2}. \quad (16)$$

The elements of the dyadics $\mathbf{V}_{\alpha\beta}$ have the form

$$V(D)_{\alpha i,\beta j} = \mathrm{Re}\left\{\sum_\mu \left(\frac{\partial \mu_\mu}{\partial x^\alpha_i}\right)_0 \left(\frac{\partial \mu_\mu}{\partial x^\beta_j}\right)_0\right\} = \mathrm{Re}\left\{\sum_\mu P^\alpha_{i\mu} P^\beta_{j\mu}\right\} \quad (17)$$

$$V(R)_{\alpha i,\beta j} = \mathrm{Re}\left\{\sum_\mu \left(\frac{\partial \mu_\mu}{\partial x^\alpha_i}\right)_0 \left(\frac{\partial m_\mu}{\partial \dot{x}^\beta_j}\right)_0\right\} = \mathrm{Re}\left\{\sum_\mu P^\alpha_{i\mu} M^\beta_{j\mu}\right\}, \quad (18)$$

where $\boldsymbol{\mu}$ stands for the electric and $\mathbf{m}$ for the magnetic dipole moment of the molecule, and $P^\alpha_{i\mu}$ and $M^\beta_{j\mu}$ are components of what is known in the VCD literature as atomic polar tensors (APTs) and atomic axial tensors (AATs), respectively. The AATs are defined according to Nafie [14]. This definition differs by a factor of $i/2\hbar$ from the one used by Stephens and coworkers [19] and in the DALTON and GAUSSIAN programs.

Computational Approach

The Cartesian harmonic force field, AATs and APTs, were all calculated at the density functional theory (DFT) level, using direct, analytical derivatives methods implemented within the GAUSSIAN program [20] and described elsewhere [19]. Our calculation uses the hybrid functionals B3PW91 and B3LYP [21] with the standard 6-311++G** [22] and aug-cc-pVDZ [23] basis sets, all available in GAUSSIAN.

Hartree–Fock linear response theory [24] and London orbitals, as implemented in the DALTON program [25], were used to compute the Raman and ROA tensors of Eqs. (9a)–(9d). They were calculated at the DFT geometry with the aug-cc-pVDZ basis set for the frequency of the exciting light, in our case 532 nm. As analytical gradients for ROA tensors are presently not available in any program, we decided to use the DALTON program, as it provides a gauge origin invariant implementation of dynamic molecular property tensors.

The displacement vectors $\mathbf{L}^x_{\alpha,p}$ of Eqs. (5), (12), and (13) were calculated with the force field from GAUSSIAN by a MATLAB [26] program developed in our laboratory. The elements of all the dyadics $\mathbf{V}_{\alpha\beta}$ [Eqs. (9a)–(9e), (17), and (18)] were also calculated by this program with gradients from DALTON for Raman and ROA and from GAUSSIAN for vibrational absorption and VCD. They were then combined with the vectors $\mathbf{L}^x_{\alpha,p}$, into the Raman and

ROA invariants [Eqs. (5) and (6)] and into the dipole and rotational strength [Eqs. (14) and (15)].

Representation of Computed Data

SPECTRA

The purpose of an ab initio calculation of VOA can be as practical as the assignment of the unknown absolute configuration of a molecule or the study of its solution conformations, by comparison of measured and computed data. Assigning absolute configurations in this way is generally cheaper than by chemical means, and far more reliable than by electronic CD or optical rotatory dispersion. In other cases, one might want to gain a better understanding of measured data with the aim of drawing conclusions of a general nature.

With the increasing precision with which ab initio calculations can be done, it has also become convenient sometimes to run a calculation, ahead of any measurement, to assess what measurable spectral features of interest one might expect for a particular molecular structure. This then allows for an informed decision as to whether undertaking a difficult and lengthy chiral synthesis may be of interest. In a case like [$^2H_1$, $^2H_2$, $^2H_3$]-neopentane, where one expects partial cancelation of VOA of opposite sign due to the close spacing of vibrational modes, the realistic simulation of experimental spectra, ahead of an arduous synthesis, is particularly important.

The careful simulation of ROA spectra is more critical than that of VCD spectra. One reason is that [$^2H_1$, $^2H_2$, $^2H_3$]-neopentane is a good Raman scatterer but a week IR absorber. Thus, the ratio of ROA to Raman intensity is expected to be smaller than the ratio of VCD to vibrational absorption. A second reason why ROA spectra merit more careful simulation than VCD spectra resides with the fact that the various terms that occur in the expressions of the scattering cross sections [Eqs. (1)–(3)] lead to bands with a differing width.

Bandwidths for isotropic Raman scattering are generally smaller than for anisotropic scattering because isotropic scattering depends on the vibrational correlation function only, while for anisotropic Raman scattering, and equally well for vibrational absorption, the orientational correlation function also comes into play. Over the past decade, rapid laser spectroscopy has made substantial contributions to the understanding of linewidths of liquid phase spectra. The classical line-broadening mechanisms, such as the Doppler effect, radiation broadening, collisions between molecules, their interaction, and their reorientation, have had to be supplanted by mechanisms such as intermolecular vibrational redistribution (IVR) [27] and vibrational dephasing by shear fluctuations [28]. A simulation of ROA spectra based on such detailed mechanisms contributing to linewidth is not possible here, notably because their importance can only be assessed by analyzing experimental data. Our aim has therefore been pragmatic, namely to account for the generally observed difference in bandwidth between isotropic and anisotropic scattering, and to explicitly include instrumental bandwidth into the simulated spectra.

To keep the problem tractable, we have made the following simplifying assumptions: (i) the instrument profile is Gaussian; (ii) the band shape of isotropic scattering is a Lorentz profile; and (iii) reorientation leads to a Lorentz profile. The band shape of anisotropic scattering, which under these assumptions is the convolution of two Lorentz curves, is therefore also a Lorentz curve.

The width of the instrument profile (full width at half-maximum [FWHM]) can be measured. For our present ROA instrument [29], the input slit is formed by fiberoptics. Thus, its width, which largely determines the resolution of the instrument, is fixed. The average value of the FWHM for the spectral range of interest was found to be 6.7 cm^{-1}. Because of the discrete nature of the CCD detector, we cannot verify that the instrument profile is truly Gaussian but, by assuming a profile, we can determine its width with reasonable precision.

The isotropic bandwidth was chosen as 3.5 cm^{-1}. This value allows us to account for the shape of the sharp, polarized Raman bands, such as the 996-cm^{-1} line of benzene, which are often observed for symmetric molecules. One must keep in mind, however, that strongly polarized bands can also have larger widths. For ROA backscattering, the choice of the isotropic linewidth is not important as isotropic scattering makes no contribution. The anisotropic width was chosen as 10 cm^{-1}.

For simulating Fourier transform VCD spectra, a 8-cm^{-1} FWHM Lorentzian line shape has often been used in the past [18]. In addition to spectra simulated with this assumption, we also present spectra obtained by the convolution of an 8-cm^{-1} Lorentz curve with the 10-cm^{-1} Gauss curve one expects for a scanning VCD spectrometer [30].

TABLE I

Parameters of the fit of Gauss curves to a Lorentz curve.

N_G		1	2	3	4	5	6	7	8
8	c_i	1.40×10^{-1}	3.71×10^{-1}	2.93×10^{-1}	1.34×10^{-1}	4.58×10^{-2}	1.25×10^{-2}	2.63×10^{-3}	3.43×10^{-4}
	a_i	2.01×10^{-1}	3.31×10^{-1}	5.61×10^{-1}	9.99×10^{-1}	$1.90 \times 10^{+0}$	$3.99 \times 10^{+0}$	$9.84 \times 10^{+0}$	$3.43 \times 10^{+1}$
7	c_i	1.83×10^{-1}	4.05×10^{-1}	2.70×10^{-1}	1.05×10^{-1}	2.98×10^{-2}	6.32×10^{-3}	8.26×10^{-4}	
	a_i	2.12×10^{-1}	3.62×10^{-1}	6.45×10^{-1}	$1.23 \times 10^{+0}$	$2.58 \times 10^{+0}$	$6.34 \times 10^{+0}$	$2.21 \times 10^{+1}$	
6	c_i	2.41×10^{-1}	4.32×10^{-1}	2.34×10^{-1}	7.37×10^{-2}	1.60×10^{-2}	2.10×10^{-3}		
	a_i	2.26×10^{-1}	4.04×10^{-1}	7.69×10^{-1}	$1.61 \times 10^{+0}$	$3.97 \times 10^{+0}$	$1.38 \times 10^{+1}$		
5	c_i	3.20×10^{-1}	4.44×10^{-1}	1.85×10^{-1}	4.34×10^{-2}	5.76×10^{-3}			
	a_i	2.43×10^{-1}	4.65×10^{-1}	9.75×10^{-1}	$2.40 \times 10^{+0}$	$8.36 \times 10^{+0}$			
4	c_i	4.26×10^{-1}	4.27×10^{-1}	1.25×10^{-1}	1.73×10^{-2}				
	a_i	2.68×10^{-1}	5.63×10^{-1}	$1.38 \times 10^{+0}$	$4.82 \times 10^{+0}$				
3	c_i	5.69×10^{-1}	3.63×10^{-1}	5.85×10^{-2}					
	a_i	3.05×10^{-1}	7.48×10^{-1}	$2.60 \times 10^{+0}$					

a_i, standard deviations of the individual Gauss curves; c_i, coefficients of the individual Gauss curves in the linear combinations.

The convolution of an instrument's Gauss profile with a Lorentz profile leads to a Voigt profile. Voigt profiles must be numerically calculated. We have decided on a different approach, namely to take advantage of the fact that the convolution of two Gauss functions is also a Gauss function.

In a first step, we have represented a Lorentz function $L(x)$ by a linear combination of Gauss functions:

$$L(x) = \frac{k^2}{x^2 + k^2} \tag{19}$$

$$L(x) \approx \sum_i c_i e^{-x^2/2a_i^2}, \tag{20}$$

where $2k$ is the FWHM of the Lorentz function with the area $F_L = k\pi$. The FWHM of the individual Gauss functions in Eq. (20) is given by $2(2 \ln 2)^{1/2} a_i$, and the area by $(2\pi)^{1/2} a_i$.

The coefficients c_i and the standard deviations a_i (Table I) were determined by fitting Gauss functions to the shape of a Lorentz function with $2k = 1$ (i.e., $F_L = \pi/2$). As can be seen from Table II, 6 Gauss functions suffice amply for representing the shape of a Lorentz curve for our spectral purposes, with the area of the approximate curve having an error of less than 1% as compared with the exact Lorentz curve. Any Lorentz curve with a FWHM of $2k$ can then be obtained as

$$L(x) \approx \sum_{i=1}^{6} c_i e^{-x^2/2(2ka_i)^2}. \tag{21}$$

In a second step, the linear combination of Gauss functions is convoluted with the Gaussian line shape function of the instrument. For the convolution of two Gauss functions one has

$$C(x) = G_a(x) \otimes G_b(x) = e^{-x^2/2a^2} \otimes e^{-x^2/2b^2} = e^{-x^2/[2(a^2+b^2)]}, \tag{22}$$

which is a Gauss function with an FWHM of $2[2 \ln 2(a^2 + b^2)]^{1/2}$ and an area of $(2\pi)^{1/2} a[1 + (b^2/a^2)]^{1/2}$.

TABLE II

Fit of Gauss curves to a Lorentz curve.

N_G	$1 - r^2$	ΔF [%]
3	3.47×10^{-4}	4.65
4	6.12×10^{-5}	2.50
5	1.28×10^{-5}	1.44
6	3.01×10^{-6}	0.86
7	7.84×10^{-7}	0.53
8	2.20×10^{-7}	0.34

ΔF, error of the area for the best least-squares fit of a linear combination of Gauss curves to the shape of a Lorentz curve. r, correlation coefficient between the two curves; N_G, number of Gauss curves used in the fit.

Hence, the convolution of the approximate Lorentz function, Eq. (21), with the instrument Gauss line shape of standard deviation b yields

$$V(x) = \frac{2}{\pi} \sum_{i=1}^{6} \frac{1}{\left[4k^2 + \left(\frac{b^2}{a_i^2}\right)\right]^{1/2}} c_i e^{-x^2/\{2[(2ka_i)^2 + b^2]\}}. \quad (23)$$

The normalized area F_V of the approximate Voigt function (23) is

$$F_V = \int_{-\infty}^{+\infty} V(x)dx = \frac{2}{\pi}(2\pi)^{1/2} \sum_{i=1}^{6} c_i a_i \approx 1. \quad (24)$$

The spectra were obtained by calculating Eq. (23) separately for the isotropic and anisotropic contributions for each vibrational band, with the areas F_V corresponding to the ab initio calculated values of the isotropic and anisotropic part of the differential scattering cross sections according to Eqs. (1), (2), and (3). The curves were then added to yield the final Raman and ROA spectra. The curves therefore represent differential scattering cross sections per steradian, and per cm^{-1}.

VIBRATIONAL MOTION, GCMS, AND ACPS

The graphic representation of vibrational motion in polyatomic non-planar molecules has been a major headache in the past, as evidenced by classical works on vibrational spectroscopy [31–33]. Except by the use of stereoscopic projections, which is inconvenient, it is difficult to simultaneously convey a good impression of the direction and the size of nuclear motion. An effective solution of the problem is to separate the two aspects [15]. The size, an isotropic quantity, can be represented by spheres centered on a molecule's nuclei, with their radius chosen proportional to the magnitude $|\mathbf{L}^x_{\alpha,p}|$ of the nuclear excursion. The direction of motion can be added by the appropriate shading of the spheres. Moreover, the surface of the spheres is then proportional to the importance of nuclear motion in generating Raman scattering and vibrational absorption.

When one is interested in the persistence of certain pattern of nuclear motion on similar fragments of different molecules [34], the energy of vibrational motion is a more important criterion. As discussed further in the section on categorizing vibrational modes, the energy of vibration of a nucleus α in mode p is proportional to $m_\alpha(\mathbf{L}^x_{\alpha,p})^2$. In representations of the distribution of vibrational energy, we have chosen the volume of spheres proportional to the contribution made by individual nuclei to the energy of a vibrational mode.

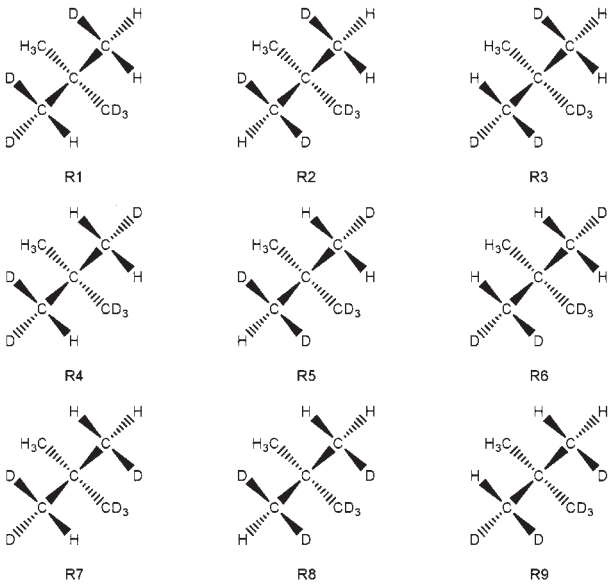

FIGURE 1. The nine rotamers of (R)-[$^2H_1$, $^2H_2$, $^2H_3$]-neopentane. Rotamers R1, R5, and R9 on the diagonal are invariant with respect to the interchange of H and D nuclei; the others are related pairwise according to Table III.

The decomposition of Raman and ROA invariants [Eq. (5)] and dipole and rotational strengths [Eqs. (12) and (13)] into mononuclear and dinuclear terms leads naturally to what we call the group coupling matrices (GCMs), which give insight into how scattering cross sections and absorption cross sections are generated within a molecule. The idea is explained in more detail in Ref. [15]. The atomic contribution patterns (ACPs) are obtained from the GCMs by splitting dinuclear terms in a meaningful way between atoms [3].

Computed Spectra

CH- AND CD-STRETCH REGION

[$^2H_1$, $^2H_2$, $^2H_3$]-neopentane has nine different conformers, which are represented in Figure 1. These rotamers have identical statistical weight,

TABLE III

Rotamers interconverted by the interchange of H and D nuclei.

Group 1	Group 2
R1	R2 ↔ R4
R5	R3 ↔ R7
R9	R6 ↔ R8

and their computed energy is so close that the experimental spectrum of liquid [$^2H_1$, $^2H_2$, $^2H_3$]-neopentane is expected to correspond to the superposition of the spectra of the individual rotamers in equal proportions.

The nine rotamers can be divided into two groups, one where the interchange of hydrogen and deuterium atoms leads to the same rotamer, and a second where it leads to a different rotamer (Table III). As an even number of nuclei is interchanged, the absolute configuration is not modified. The property that the interchange of isotopic nuclei leads to the same enantiomer of a molecule is not unique to [$^2H_1$, $^2H_2$, $^2H_3$]-neopentane. It also pertains to a compound like 1,3-dideuterionallene. Likewise, other chiral molecules with two distinct groups of conformers, one that does have this property and another where it is absent, can be thought of, but stereochemists do not seem to have discussed this aspect of molecules chiral by isotope substitution. [$^2H_1$, $^2H_2$, $^2H_3$]-neopentane can certainly be considered the prototype and the smallest of the molecules where this is possible.

Naively, one might think that the three rotamers 1, 5, and 9, where hydrogen and deuterium nuclei occupy equivalent sites, must lead to identical VOA, except for size, for vibrations where either the H nuclei, or the D nuclei, move in the same coupled motion, independent of the other nuclei of the molecule. Vibrations that satisfy this criterion are the CH- and the CD-stretch vibrations. The expected similarity of the VOA of the two spectral regions is not borne out for the antisymmetric stretch vibrations of rotamers 1 and 5, as can be seen from the line spectra in Figure 2. Rather, upon more careful inspection, it turns out that pairs of antisymmetric CH- and CD-stretch vibrations with the same nuclear motion for H and D nuclei, i.e., 45 and 39, and 43 and 37, represent textbook examples for a situation where inertial contributions, rather than coupling of nuclear motion, determine VOA spectra.

The existence of inertial contributions can best be appreciated by first assuming that all hydrogen and deuterium nuclei do actually move in precisely the same way, with an interchanged role, in high- and low-energy sister vibrations. It is then obvious that the Sayvetz conditions cannot, in general, be satisfied simultaneously for both vibrations, because of the differing mass of the H and D nuclei. Thus, even if the motion of the two types of nuclei looks similar, except for the smaller size of the amplitudes of the D atoms, sister vibrations must differ. For rotamers 1 and 5, the calculations show that this difference is sufficiently pronounced as to lead to an opposite sign for ROA as well as VCD.

The same is true for all rotamers of group 2 without exception, where the VOA of sister vibrations has to be compared for pairs of rotamers

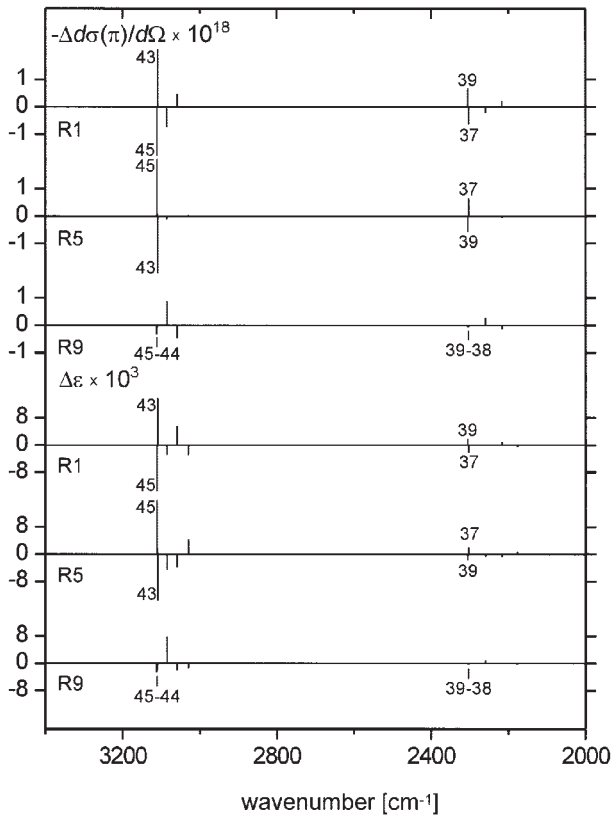

FIGURE 2. ROA backscattering and VCD line spectra of the CH- and CD-stretch region of the rotamers of (R)-[$^2H_1$, $^2H_2$, $^2H_3$]-neopentane invariant to H/D interchange. Vertical scales: ROA: [Å^2 sr^{-1}], VCD: [10^3 cm^2 mol^{-1}]. Force field for all spectra: DFT with B3PW91 hybrid functional and aug-cc-pVDZ basis set. VCD electronic tensors: same as force field. ROA electronic tensors: TDHF with aug-cc-pVDZ basis set.

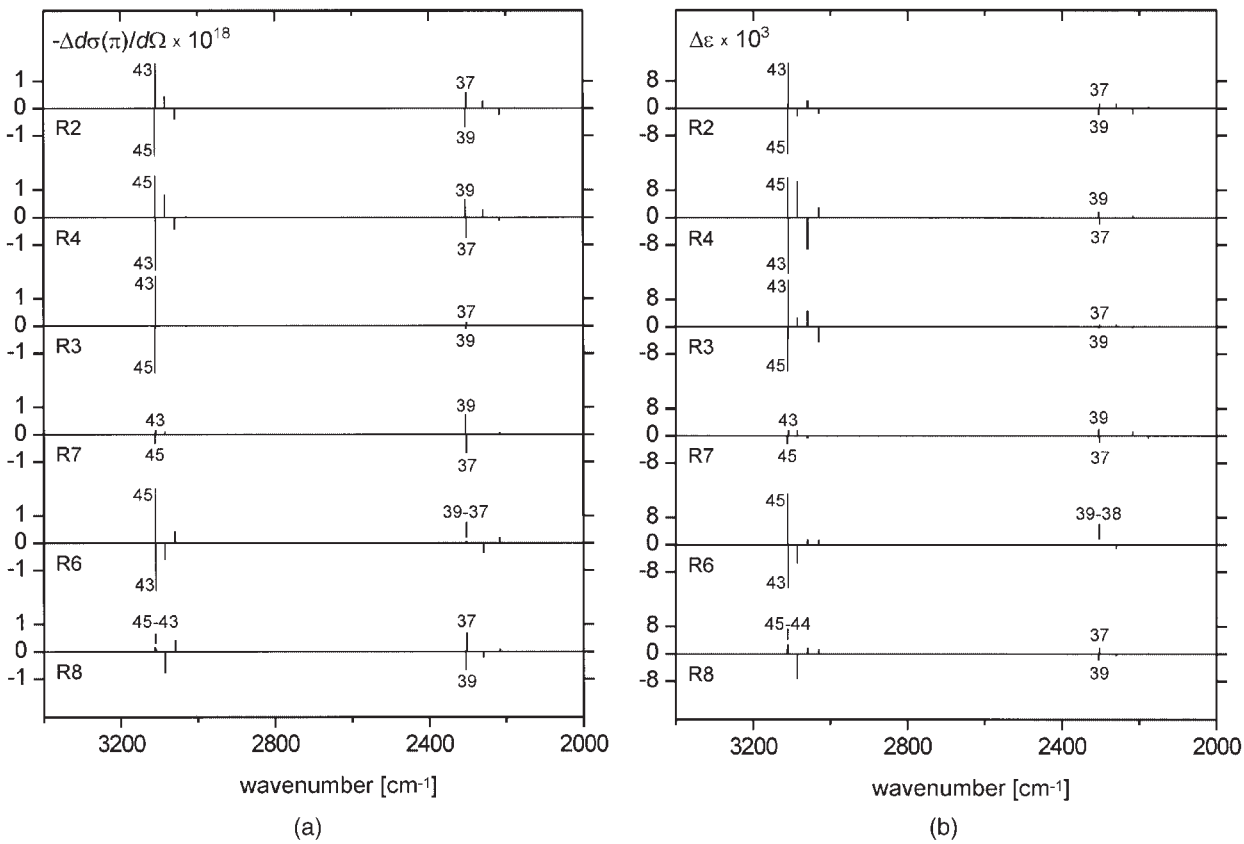

FIGURE 3. (a) ROA backscattering line spectra of the CH- and CD-stretch region of the rotamers of (R)-[$^2H_1$, $^2H_2$, $^2H_3$]-neopentane not invariant to H/D interchange. Pairs of interconverted rotamers are grouped. Vertical scale: [Å^2 sr^{-1}]. Computational parameters: as in Fig. 2. (b) VCD line spectra of the CH- and CD-stretch region of the rotamers of (R)-[$^2H_1$, $^2H_2$, $^2H_3$]-neopentane not invariant to H/D interchange. Pairs of interconverted rotamers are grouped. Vertical scale: [10^3 cm^2 mol^{-1}]. Computational parameters: as in Fig. 2.

according to Table III; i.e., one has to compare the VOA of the antisymmetric CH-stretch vibration 45 of rotamer 2 with the VOA of the antisymmetric CD-stretch vibration 39 of rotamer 4, and vice versa. The ROA line spectra, grouped for pairs of rotamers, are shown in Figure 3(a) and the VCD spectra in Figure 3(b). The vibrations 45 and 39, and 43 and 37, are invariably coupled antisymmetric vibrations spread over two methyl groups in the way shown in Figure 4 for rotamer 5. The antisymmetric stretch vibrations 44 and 38, which are not discussed further, are located on a single methyl group and show small VOA.

The group coupling matrices for sister vibrations show identical sign pattern, as one would expect for vibrations with such a similar appearance. The exception are matrix elements with the nucleus at position e in Figure 4, which is occupied by hydrogen in mode 45 and 43, and deuterium in 39 and 37, and which moves in sister vibrations with an opposite phase, relative to other nuclei. This is clearly visible in Figure 4, which, for the sake of clarity, reproduces only a small fragment of the complete atomic GCM. It is not, however, actually the contributions of site e by themselves that determine the sign of 39 relative to 45, and 37 relative to 43. Rather, the relative size of all the major positive and negative matrix elements changes systematically. It is through this that the influence of inertial contributions is manifested.

The relative size of the ROA and VCD for the CH-stretch and CD-stretch region can be understood. ROA and VCD are proportional to the square of $\mathbf{L}^x_{\alpha,p}$, according to Eqs. (5) and (13), and for vibrations where the H or D nuclei only move, the square of $\mathbf{L}^x_{\alpha,p}$ is inversely proportional to the mass m_α of these nuclei, according to Eq. (8). In reality, the size of $\mathbf{L}^x_{\alpha,p}$ will be additionally reduced for the

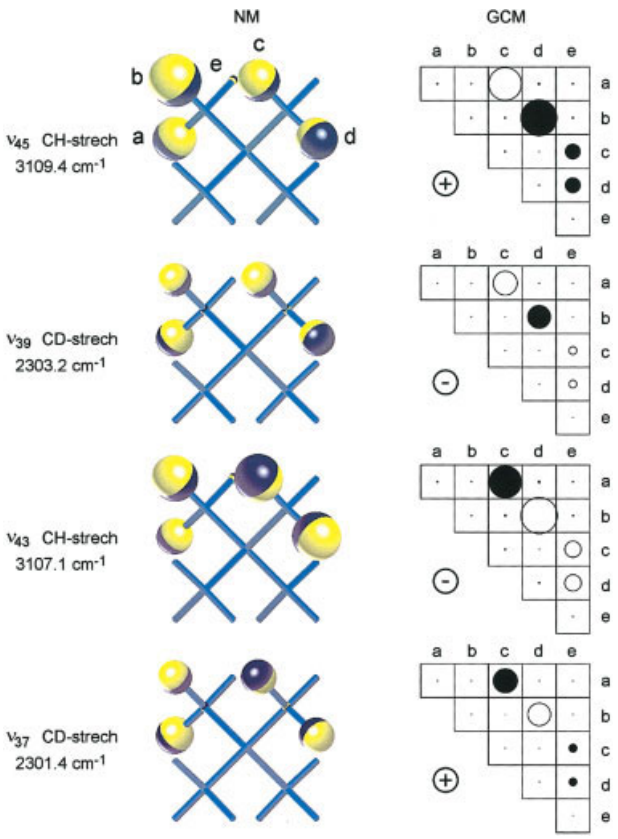

FIGURE 4. Antisymmetric CH- and CD-stretch vibrations 45, 39, and 43, 37 of rotamer 5. For clarity, the group coupling matrices include only the five nuclei that make the largest contributions. Site **e** is the only one for which the relative phase of motion changes upon an interchange of H and D nuclei. Sites **a**, **b**, **c**, **d**, and **e** are occupied by H nuclei for vibrations 45 and 43, and by D nuclei for vibrations 39 and 37. Black circles: positive, open circles: negative. Computational parameters: as in Fig. 2. [Color figure can be viewed in the online issue, which is available at www.interscience.wiley.com.]

CD-stretch region by a larger contribution from carbon nuclei. This favors ROA and VCD in the CH-stretch region. In contrast, ROA, but not VCD, is disfavored in the CH-stretch region by a factor $\Delta\omega_{CD}/\Delta\omega_{CH}$, and by the dependence of K_p, Eq. (4), on the frequency ω_p of the scattered light. The difference in size in the CH-stretch and the CD-stretch region is therefore less pronounced for ROA than for VCD.

The signs of the ROA line spectra show a remarkable similarity to that of the VCD spectra in the CH- and the CD-stretch region, for all nine rotamers. This is of interest for two reasons. For one, ROA and VCD are defined with differing sign conventions: ROA as proportional to the number of right minus left circularly polarized photons removed by scattering from light traversing a sample, and VCD as proportional to the number of left minus right circularly polarized photons removed by absorption. For another, it has so far been found that there is no relation [35] between ROA and VCD spectra. While this is certainly often true, our results also show that such a relation can exist. The fact that for CH- and CD-stretch vibrations of [$^2H_1$, $^2H_2$, $^2H_3$]-neopentane the ROA and the VCD show the same sign is most likely a consequence of their being determined by inertial contributions, but this will have to be investigated in more detail. As will be seen later, for the lower-energy regions, the sign of ROA and VCD is predominantly opposite.

The diagram in Figure 5 shows the energy of the CH- and CD-stretch vibrations of [$^2H_1$, $^2H_2$, $^2H_3$]-neopentane, relative to that of undeuterated and fully deuterated neopentane. These latter molecules have 12 CH- and CD-stretch vibrations, respectively, with eight modes representing linear combinations of the doubly degenerate antisymmetric stretch vibrations of the four methyl groups, and four modes combinations of symmetric methyl stretch vibrations. In [$^2H_1$, $^2H_2$, $^2H_3$]-neopentane,

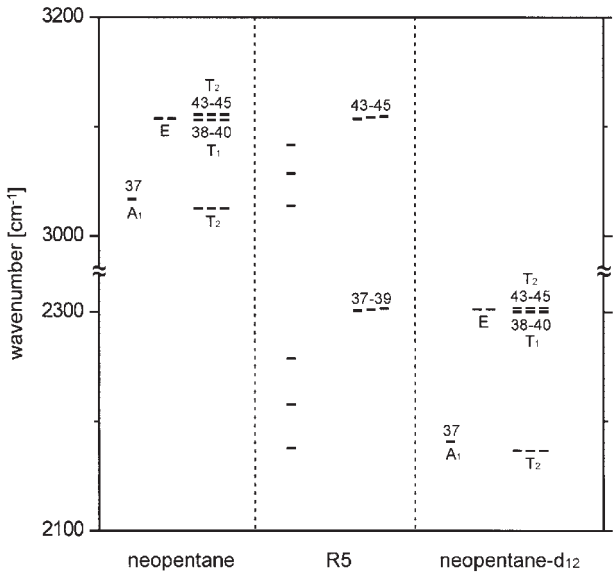

FIGURE 5. Diagrammatic representation of the energy levels of the CH- and the CD-stretch modes of neopentane, rotamer 5 of [$^2H_1$, $^2H_2$, $^2H_3$]-neopentane, and perdeuterated neopentane. Computational parameters: as in Fig. 2.

the four CH-stretch vibrations of highest energy go back to the antisymmetric CH-stretch vibrations of the undeuterated molecule. Three of them have been discussed in a previous paragraph, and the fourth is a simple CH-stretch motion of the lonely H nucleus of the CHD_2 group. The two symmetric CH-stretch vibrations occur at lower energy and are localized on the CDH_2 and the CH_3 group, respectively. The CD-stretching vibrations follow the same pattern.

According to our calculations with a harmonic force field, the ROA and the VCD of individual rotamers would be measurable in the CH- and CD-stretch region but, as shown in Figures 6 and 7, not for their mixture, because of dilution and extensive cancelation. Direct frequency shifts due to anharmonicity are not likely to have much influence on cancelation, as different rotamers are expected to be similarly affected. Less predictable is the indirect influence that anharmonicity can have on the energy of CH- and CD-stretch vibrations through Fermi resonances. The energy of lower-frequency modes, the overtones and combination frequencies of which are relevant to Fermi resonance, varies from one rotamer to another. This is an aspect of considerable interest, but it is outside the scope of the present work.

LOWER FREQUENCY REGION

At $<$1,600 cm^{-1}, the ROA and VCD of [$^2H_1$, $^2H_2$, $^2H_3$]-neopentane should both be measurable for the mixture of rotamers, as is evident from Figures 6 and 7. The effect of dilution and cancelation can be estimated from comparison of the line and band spectra of the Δ-values for ROA and g-values for VCD. These quantities are defined as

$$\Delta = \frac{I_R - I_L}{I_R + I_L} \tag{25}$$

$$g = \frac{2(\varepsilon_L - \varepsilon_R)}{\varepsilon_L + \varepsilon_R}. \tag{26}$$

The line spectra reflect Δ- and g-values for individual rotamers, while the band spectra correspond to the ratio of the difference to the sum spectra obtained by summing the band spectra of individual rotamers.

Δ and g can be used to judge the measurability of VOA. For ROA, the value of Δ should, with present instrumentation, be $\sim>10^{-5}$ as otherwise measurements become difficult or impossible. This limitation is due to offsets caused by straylight and multiple reflections between optical elements, which can be present even in a spectrometer with advanced offset compensation [36]. According to Figure 6, more than a dozen of the ROA bands in the 700–1,400-cm^{-1} range have Δ-values that satisfy this condition easily. The minimum amount of substance required in backscattering, to which Figure 6 applies, is of the order of 2–4 mg, but it can be reduced to $<$1 mg in right angle scattering [1].

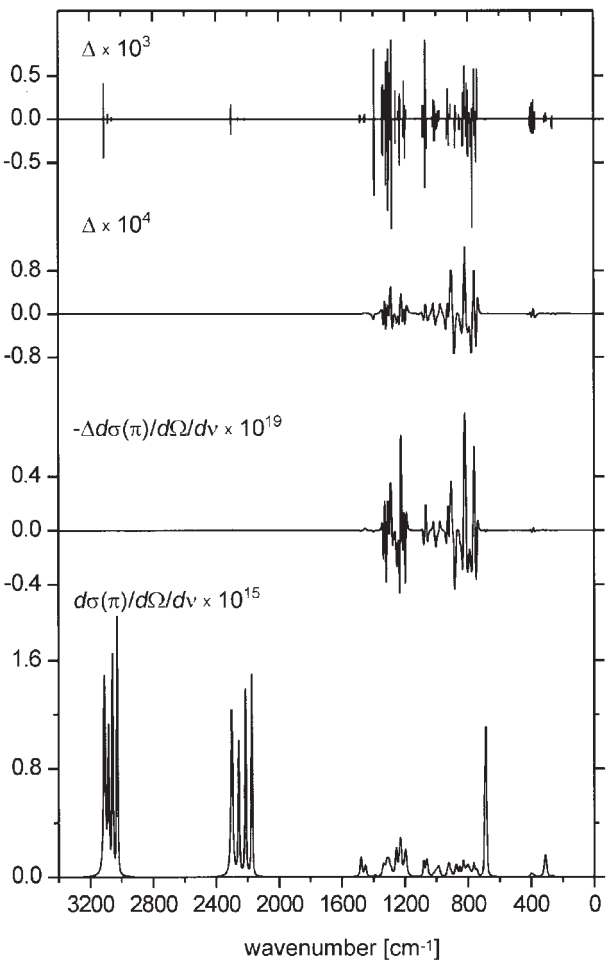

FIGURE 6. Backscattering Raman and ROA spectra of the mixture of the nine rotamers of (R)-[$^2H_1$, $^2H_2$, $^2H_3$]-neopentane. From bottom to top: Raman, ROA, ratio of ROA to Raman, line spectrum of Δ-values of individual vibrations. Band shapes: isotropic, 3.5 cm^{-1} FWHM Lorentz convoluted with 6.7 cm^{-1} FWHM Gauss; anisotropic, 10 cm^{-1} FWHM Lorentz convoluted with 6.7 cm^{-1} FWHM Gauss. Units for the representation of scattering cross sections: [$Å^2$ sr^{-1} cm]. Computational parameters: as in Fig. 2.

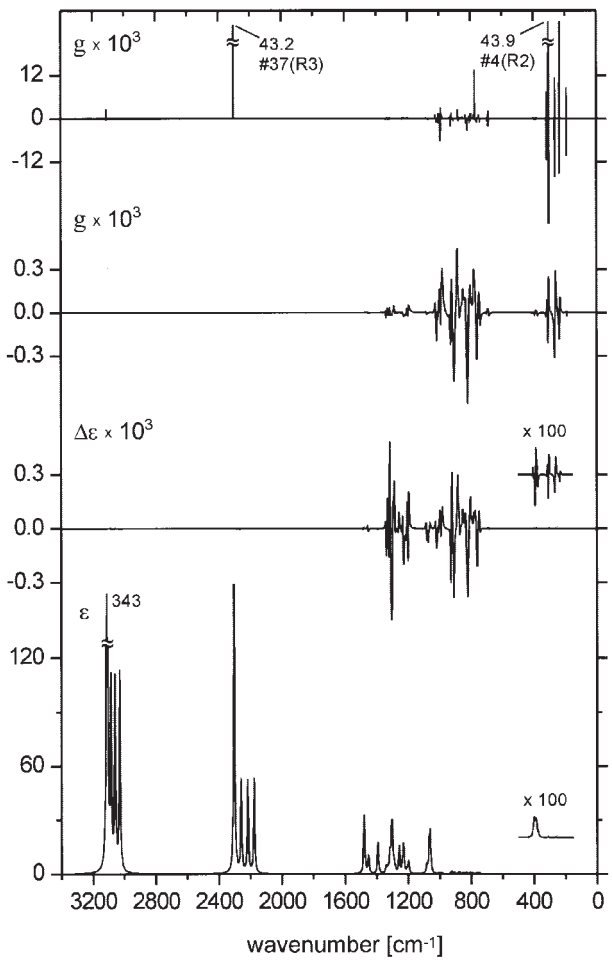

FIGURE 7. Vibrational absorption and VCD spectra of the mixture of the nine rotamers of (R)-[$^2H_1$, $^2H_2$, $^2H_3$]-neopentane. From bottom to top: absorption, VCD, ratio of VCD to absorption, line spectrum of *g*-values of individual vibrations. A Lorentzian line shape with an FWHM of 8 cm^{-1} was used for all bands. Exceptionally large *g*-values in the line spectrum are due to modes with negligible absorption. Units of extinction coefficients: [10^3 cm^2 mol^{-1}]. Computational parameters: as in Fig. 2.

The conditions for the measurability of VCD are similar to ROA. One advantage of VCD over ROA is that weak absorption can be compensated for by a longer path length of the measurement cell. This does, of course, require more substance than the usual 50 mg, already far in excess of what is needed for ROA. In contrast, VCD should be easier to measure as the *g*-values calculated for the 700–1,000-cm^{-1} region are much larger than the Δ-values for ROA. The reason is not that the VCD as such is large for [$^2H_1$, $^2H_2$, $^2H_3$]-neopentane, but rather that IR absorption at <1,000 cm^{-1} is very small for this nonpolar molecule, and exceedingly small at <400 cm^{-1}. This latter spectral region, which is dominated by methyl torsional motion, is, at present, out of reach for VCD.

Two silent modes of individual rotamers, i.e., 37 for R3 at 2,303 cm^{-1} and 4 for R2 at 303 cm^{-1}, show *g*-values of more than 4%, which is extraordinary for VCD.

Figure 8 shows the influence of instrumental res-

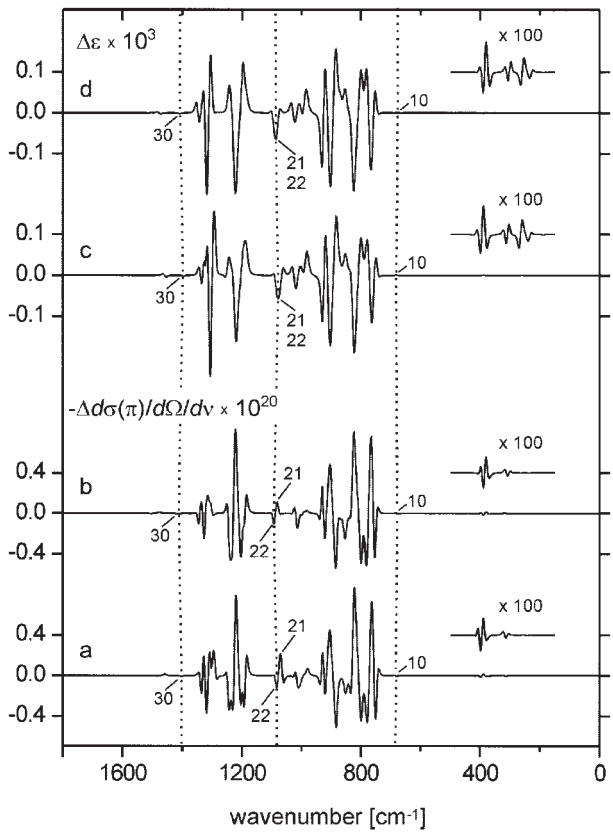

FIGURE 8. Influence of line shape and computational parameters on computed spectra of the mixture of rotamers. ROA spectra **a** and **b**: line shape as in Fig. 6. VCD spectra **c** and **d**: 8 cm^{-1} FWHM Lorentz curve convoluted with 10 cm^{-1} Gauss curve. **a**: DFT/B3LYP/aug-cc-pVDZ force field, TDHF/aug-cc-pVDZ electronic tensors. **b**: DFT/B3LYP/6-311++G** force field, TDHF/aug-cc-pVDZ electronic tensors. **c**: DFT/B3LYP/aug-cc-pVDZ force field and electronic tensors. **d**: DFT/B3LYP/6-311++G** force field and electronic tensors. Broken vertical lines indicate the position of the molecular breathing mode 10, the CD_3 umbrella mode 22, and the CH_3 umbrella mode 30, which delimit the spectral regions of large VOA. Units of scattering cross sections and extinction coefficients: as in Figs. 6 and 7.

olution on measured VCD. The pure Lorentzian band shape of an FWHM of 8 cm^{-1} used in Figure 7 was convoluted as described earlier with the 10-cm^{-1} FWHM Gaussian resolution curve typical for a scanning VCD instrument. Clearly, the size of the VCD is reduced, and its appearance somewhat modified, but there is no doubt that, given enough substance, the VCD of [$^2H_1$, $^2H_2$, $^2H_3$]-neopentane should remain easily measurable.

As a further check of the validity of our assessment of the measurability of the ROA and VCD of [$^2H_1$, $^2H_2$, $^2H_3$]-neopentane, we have repeated the calculations with a different functional and a different basis set, namely B3LYP and 6-311++G**. Again, as seen in Figure 8, the measurability of the molecule's VOA is confirmed.

Sorting Vibrational Modes

Traditionally, vibrational modes have been characterized by looking at internal coordinates such as the bending of valence angles, the deformation of torsional angles, and bond stretching. Where a vibration is located primarily on a small molecular fragment, internal coordinates are an immensely practical way of categorizing nuclear motion. In analytical applications of vibrational spectroscopy, in particular, the notion of group vibrations, such as the carbonyl stretching vibration, and the notion of spectral regions, such as amide I and II, are of key importance. The approach is less useful for skeletal modes extending over sizable portions of a molecule, and quite generally for vibrations of the so called fingerprint region. It is typically these spectral regions that are of particular interest in VOA, and both have only become computationally accessible through the advent of ab initio methods.

The classical approach for categorizing molecular vibrations also reaches somewhat its limits for a molecule such as [$^2H_1$, $^2H_2$, $^2H_3$]-neopentane, for which four methyl groups are the only distinct molecular fragments. This has been an incentive for us to look for additional means for distinguishing molecular vibrations, and in particular for measures directly adapted to the ab initio computation of normal modes in Cartesian coordinates.

The decomposition of the potential energy of a vibration into components attributable to internal coordinates has been used in the past [37]. We suggest as an alternative measure the decomposition of the total energy of vibration into individual nuclear components. The vibrational energy can be decomposed in mononuclear terms by looking at the kinetic energy, rather than the potential energy, because the kinetic energy of a normal mode Q_p is the sum of the kinetic energies of the individual nuclei α,

$$T_p = \frac{1}{2}\dot{Q}_p^2 = \sum_\alpha T_{\alpha,p} = \frac{1}{2}\sum_\alpha m_\alpha \Delta\dot{\mathbf{x}}_{\alpha,p}\cdot\Delta\dot{\mathbf{x}}_{\alpha,p} = \frac{1}{2}\dot{Q}_p^2\sum_\alpha m_\alpha \mathbf{L}^x_{\alpha,p}\cdot\mathbf{L}^x_{\alpha,p}, \quad (27)$$

where $\Delta\mathbf{x}_\alpha = \mathbf{L}^x_{\alpha,p}Q_p$ has been used. According to the virial theorem, $V_p = T_p = E_p/2$. In a normal vibration, all nuclei execute a harmonic motion with the same frequency and phase, which means that the effective potential seen by each nucleus must be harmonic. One can therefore also set $V_{\alpha,p} = T_{\alpha,p}$. This effective potential is the sum of the local potential of the nucleus and the potential produced by the pushing and pulling of all other nuclei. Thus, the fraction of vibrational energy $E_{\alpha,p}$ which nucleus α contributes to normal mode p can be written as:

$$\frac{E_{\alpha,p}}{E_p} = m_\alpha \mathbf{L}^x_{\alpha,p}\cdot\mathbf{L}^x_{\alpha,p}. \quad (28)$$

By summing the contributions of individual nuclei, one can define the vibrational energy of a molecular fragment, or of a particular kind of nuclei. It is the latter approach that is used in this case.

Another useful means for distinguishing modes is to look at the difference of the distance between nuclei for the two turning points of nuclear motion. The sum of distance changes can be defined for the whole molecule, for molecular fragments, or between molecular fragments, in a completely analogous fashion as discussed for group coupling matrices [15], except that mono-nuclear terms are, of course, inherently zero.

Figure 9 shows the decomposition of the vibrational energy into separate components attributable to carbon, deuterium, and hydrogen atoms for neopentane, and for fully and partially deuterated neopentane, with rotamer 5 chosen as the example. The change of the sum of all distances between nuclei is displayed in Figure 10. The Raman spectra of the symmetric molecules are shown together with the degree of circularity [13, 29] in Figure 11, and the Raman and ROA spectra for the nonsymmetric one in Figure 12.

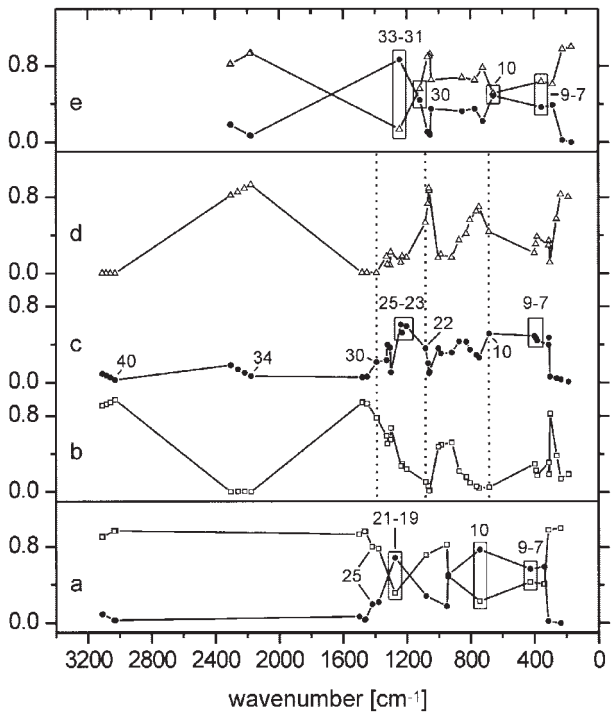

FIGURE 9. Vibrational energy distribution diagrams calculated according to Eq. (28). Bottom: neopentane. Middle: rotamer 5 of [$^2H_1$, $^2H_2$, $^2H_3$]-neopentane. Top: perdeuterated neopentane. Vertical broken lines separate the same spectral regions as in Fig. 8. ●, carbon; □, hydrogen; △, deuterium atoms. Computational parameters: as in Fig. 2.

Figure 10 is easiest to interpret. For the two symmetric molecules, the sum of all distances differs from zero only for the three vibrations of A_1 symmetry, i.e., the molecular breathing mode, the totally symmetric umbrella or symmetric CH_3/CD_3 deformation mode, and the totally symmetric CH_3/CD_3 stretching mode. Raman scattering for these A_1 symmetric vibrations is fully polarized, which means a degree of circularity of -1 in Figure 11. In contrast to the stretching and breathing motions, the Raman scattering intensity of the A_1 umbrella mode is weak, however, and for neopentane it would not be identifiable separately in the experimental Raman spectrum.

The small Raman scattering intensity is a general, and so far not well understood, characteristic of the CH_3 umbrella mode. The reason is cancelation between positive mononuclear and negative dinuclear terms on individual CH_3 groups, as can be seen from the GCMs in Figure 13. The cancelation is less pronounced for the CD_3 group, despite its identical electronic structure. Additionally, mononuclear contributions by carbon atoms also make a larger contribution. CD_3 groups therefore lead to more scattering than CH_3 groups. For vibrational absorption, the situation is the opposite: absorption by the umbrella mode of individual methyl groups is substantial [33], and most of it is due to the hydrogen and not the carbon atoms, as seen from Figure 13. In contrast, the umbrella motion of CD_3 groups produces less absorption than that of CH_3 groups. In the symmetric molecules, the total absorption intensity vanishes, of course, for the A_1 symmetric mode, because of exact cancelation between methyl groups.

In [$^2H_1$, $^2H_2$, $^2H_3$]-neopentane, the isolated umbrella mode 22 of the single CD_3 group shows a fair amount of mixing with other modes, the umbrella mode 30 of the CH_3 group very little. The umbrella mode of the CD_3 group contributes substantially to the negative VCD band just below 1,200 cm^{-1} in the spectra for the mixture of rotamers in Figure 8. It

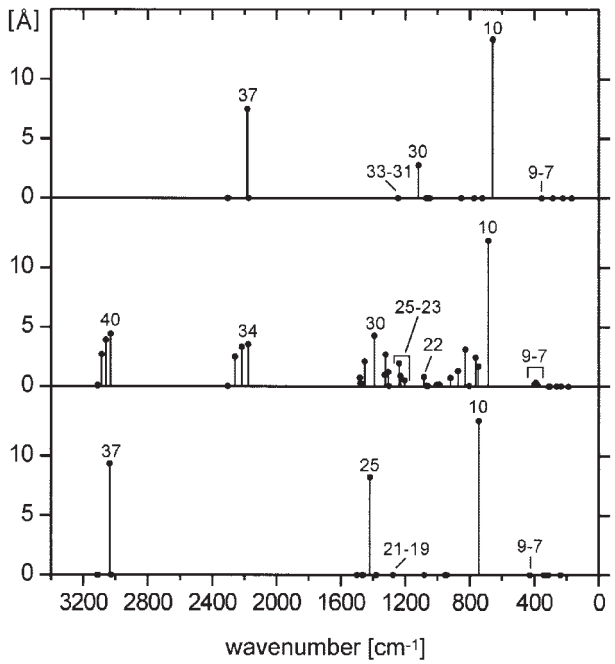

FIGURE 10. Variation of the sum of internuclear distances with vibrational motion. The magnitude of the difference of the sums of all internuclear distances is shown for the two classical turning points of nuclear motion, with zero point vibrational amplitudes. Bottom: neopentane. Middle: rotamer 5 of [$^2H_1$, $^2H_2$, $^2H_3$]-neopentane. Top: perdeuterated neopentane. Only modes of symmetry species A_1 produce a change for the two symmetric molecules. Force field: as in Fig. 2.

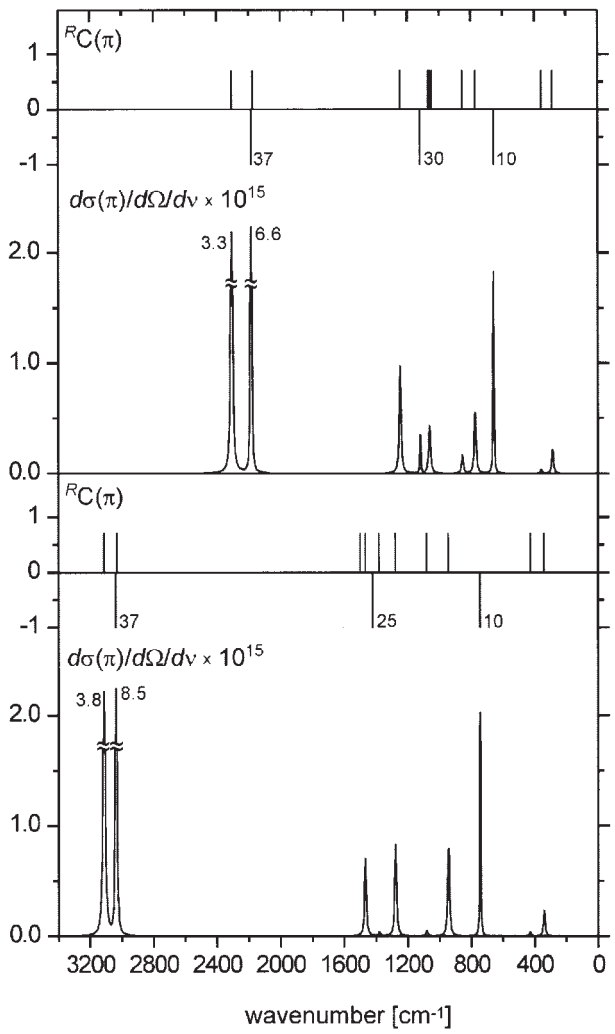

FIGURE 11. Backscattering Raman spectrum of neopentane (bottom half) and perdeuterated neopentane (top half). The line spectra indicate the degree of circularity. Vibrations of species A_1 have $C(\pi) = -1$, vibrations of species T_2 and E have $C(\pi) = 5/7$, vibrations of species T_1 and A_2 are silent. Bandwidths and units of scattering cross sections: as in Fig. 6. Computational parameters: as in Fig. 2.

can be easily identified in the energy decomposition diagram (Fig. 9) by its low H, high D, and substantial C energy content. In contrast, the VCD signal of the umbrella vibration 30 of the CH_3 group is negligible.

The degree of mixing, in the partially deuterated molecule, of the A_1 symmetric modes of neopentane and of fully deuterated neopentane with modes of other symmetry species, is evidenced by the nonzero value of the sum of the internuclear distances of most modes. Notable exceptions are the lowest-energy torsional vibrations, and the three highest-energy vibrations of the antisymmetric CH- and CD-stretch type. If compared with their parent vibrations of the symmetric molecules, even these modes appear strongly modified, however, less by the character of the motion of the H and D atoms on individual methyl groups than by the change of coupling between methyl groups. In the torsional modes, which are the four lowest-energy modes of the molecule, the CD_3, CD_2H, CDH_2, and CH_3 group execute their motions largely independently from each other. Their motion cannot be completely independent, however, notably because of the Sayvetz conditions. This is visible from the energy decomposition diagram in Figure 9, which shows that the D energy content of the second to lowest torsional motion is actually slightly higher than in the lowest one.

The spectral region with substantial VOA in Figure 8 is bound at the lower end by the molecular

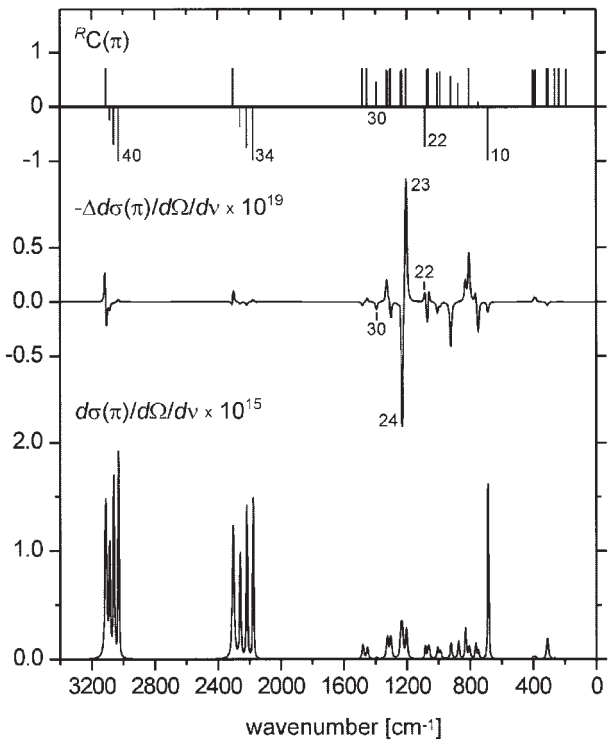

FIGURE 12. Backscattering Raman and ROA spectra of rotamer 5 of (R)-[$^2H_1$, $^2H_2$, $^2H_3$]-neopentane. The line spectrum indicates the degree of circularity of individual Raman bands. Bandwidths and units of scattering cross sections: as in Fig. 6. Computational parameters: as in Fig. 2.

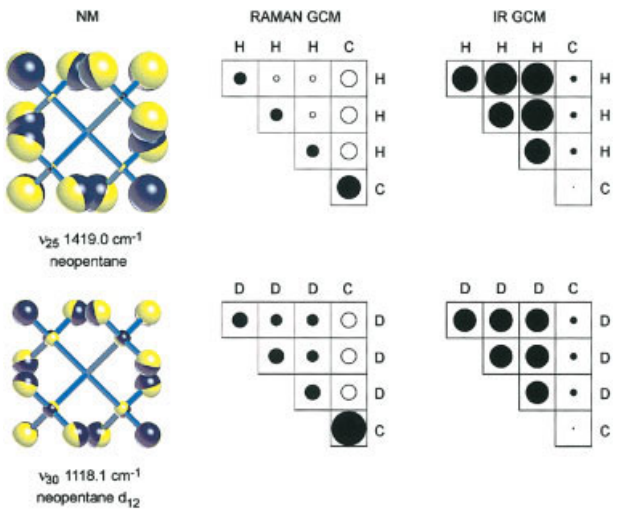

FIGURE 13. Umbrella mode of species A_1 of neopentane and perdeuterated neopentane. Columns and rows of the group coupling matrices correspond to the H or D, and the C atoms of individual methyl groups. For neopentane, the total vibrational absorption intensity of the A_1 mode vanishes due to canceling terms between methyl groups. Black circles, positive; open circles, negative. Computational parameters: as in Fig. 2. [Color figure can be viewed in the online issue, which is available at www.interscience.wiley.com.]

breathing mode 10 at 685 cm^{-1}, and at the higher end by the CH_3 umbrella mode 30 at 1,391 cm^{-1}. There is little ROA and VCD outside these bounds, contrary perhaps to what one might expect for the CCC bending and twisting motions at energy of $<$685 cm^{-1}. The observation agrees with our experience for other molecules chiral by deuterium substitution.

Moreover, from Figures 8 and 12, it is evident that the main region of VOA activity falls into a lower- and a higher-energy section, to the right and left, respectively, of the CD_3 umbrella mode 22, found at 1,084 cm^{-1} in rotamer 5. In the lower-energy section, 685–1,084 cm^{-1}, the rocking motion of whole methyl groups, and their deformation motions, dominate, with the energy distribution gradually shifting from D to H with increasing total energy. In the higher-energy section, 1,084–1,391 cm^{-1}, CC-stretching motion comes into play. The three CC-stretching vibrations 23–25, identified by numbering in Figure 14, have a high carbon content and produce substantial ROA in all rotamers. Figure 15 displays the nuclear motion of vibration 23 and 24, which are responsible for the large couplet in the ROA spectrum of rotamer 5 in Figure 12. The parent vibrations in the symmetric molecules are the T_2 symmetric modes 19–21 in neopentane and 31–33 in perdeuterated neopentane. This triplet of vibrations can be easily identified for the three molecules in the energy level diagram of Figure 14.

Comparison of the ROA and the VCD spectra of Figure 8 shows that they are close to mirror images of each other. This is contrary to what we found for the CH- and CD-stretch region dominated by inertial contributions, and is one of the unexpected features of the VOA of [$^2H_1$, $^2H_2$, $^2H_3$]-neopentane. The mirror image aspect, which is far too pronounced to represent a statistical fluke, is more easily visible for the mixture of rotamers than for individual rotamers. A detailed analysis will have to show why this is so, as well as what conclusions

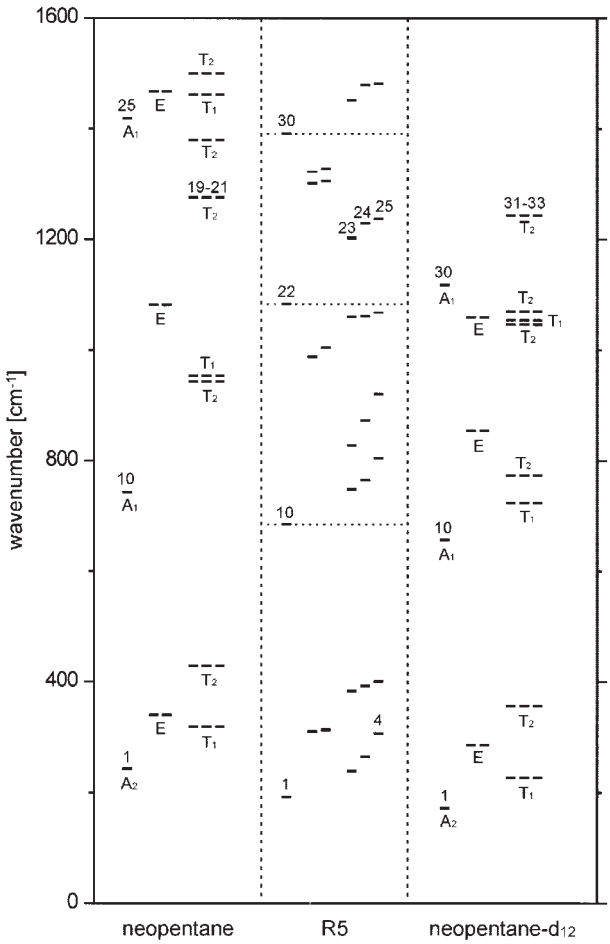

FIGURE 14. Diagrammatic representation of the energy levels of the lower frequency modes of neopentane, rotamer 5 of [$^2H_1$, $^2H_2$, $^2H_3$]-neopentane, and perdeuterated neopentane. Computational parameters: as in Fig. 2.

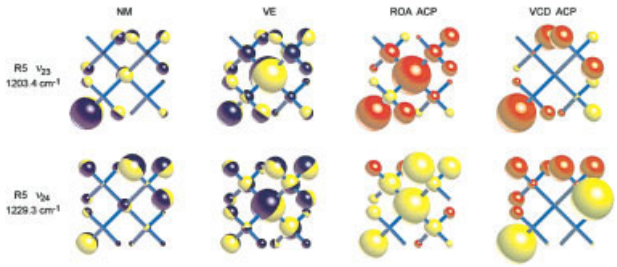

FIGURE 15. Representation of the displacements (NM) and the vibrational energies (VE) of individual nuclei in modes 23 and 24 of rotamer 5 of (R)-[$^2H_1$, $^2H_2$, $^2H_3$]-neopentane, with the ROA and VCD atomic contribution pattern generated by these vibrations. Red circles, positive; yellow circles, negative. Computational parameters: as in Fig. 2. [Color figure can be viewed in the online issue, which is available at www.interscience.wiley.com.]

can be drawn from it for the VOA of other molecules.

Summed VOA Intensities

A striking aspect of all VOA spectra is the fact that positive and negative contributions appear to cancel over an entire spectrum. This is particularly visible in ROA spectra because they can be measured over a more extended spectral range than VCD spectra. In electronic optical activity, according to a well-known sum rule, the value of the rotational strengths summed over all transitions between the ground state and electronically excited states vanishes [38]. In VOA, the analogous sum over the excited states of a particular vibrational mode is of little interest, as it is the VOA for fundamental transitions, summed over all vibrational modes, that can be measured. Cuony and Hug [39] showed that a general rule for the value of the ROA summed over vibrational modes does not exist, even though this sum (if it is extended to include all normal modes, which also means those with zero vibrational frequency corresponding to translational and rotational motion) does vanish for certain molecules that owe their chirality to isotope substitution. For VCD, Buckingham [16] has more recently discussed the balancing of summed positive and negative VCD contributions for fundamental vibrational transitions by using the argument that nondegenerate vibrational levels cannot support a time-odd property, such as a magnetic moment.

The significance of the small but definite nonzero size of the sum of total vibrational ROA intensity, obtained by adding the ROA of individual vibrational modes multiplied by appropriate frequency factors, has only recently been understood [3]. It is a measure of the chirality of the electron distribution, as seen by the nuclei when they move in the various normal modes of a molecule. [$^2H_1$, $^2H_2$, $^2H_3$]-neopentane, with its T_d symmetric electron distribution, is the perfect molecule for numerically testing this as it can be argued that its summed vibrational ROA should be negligible.

Summing individual terms in Eq. (5) over all normal modes, including those with zero frequency, yields an expression independent of the normal coordinates $\mathbf{L}^x_{\alpha,p}$:

$$\sum_p^{NM} \mathbf{L}^x_{\alpha,p} \cdot \mathbf{V}_{\alpha\beta} \cdot \mathbf{L}^x_{\beta,p} = \sum_p^{NM} \sum_{i,j} V_{\alpha i,\beta j} L^x_{\alpha i,p} L^x_{\beta j,p}$$
$$= \sum_{i,j} V_{\alpha i,\beta j} m_\alpha^{-1} \delta_{\alpha i,\beta j} = \sum_i V_{\alpha i,\alpha i} m_\alpha^{-1} \delta_{\alpha\beta} = V_\alpha m_\alpha^{-1} \delta_{\alpha\beta}, \quad (29)$$

where NM means summation over all normal modes, and where

$$V_\alpha = \sum_i V_{\alpha i,\alpha i}. \quad (30)$$

V_α is a purely electronic quantity. For Raman and vibrational absorption, it is a true scalar, but for ROA and VCD, as an invariant combination of the elements of a true and of a pseudo-second-rank tensor, it is a pseudo-scalar. Consequently, for a nucleus located in a mirror plane of a molecule's electron distribution, V_α vanishes, and for two nuclei α and β located at enantiotopic sites, $V_\beta = -V_\alpha$ [39]. Thus, for ROA and VCD the sum (29) vanishes for a molecule such as [$^2H_1$, $^2H_2$, $^2H_3$]-neopentane, where all nuclei are located in mirror planes of the electron distribution. In molecules with a less symmetric electron distribution, (29) will not, in general, vanish for ROA, but it does vanish for VCD unless the molecule supports a permanent magnetic dipole moment [16].

Translational motion does not lead to ROA. Equation (29) therefore represents a rovibrational sum. It is possible to subtract the rotational contribution and to obtain a measure for the vibrational part alone, which then can be directly compared with the sum of measured vibrational ROA inten-

sities, provided individual measured bands are multiplied by appropriate frequency factors. For this purpose, it is best to define a fractional, dimensionless measure [3], as it is difficult to measure absolute Raman scattering cross sections. For ROA backscattering, one can write for the fractional contribution of a molecule's chiral electron distribution to rovibrational Raman scattering:

$$\delta(\text{rovib}) = \frac{\sum_\alpha [12V(\beta^2_G)_\alpha + 4V(\beta^2_{\mathcal{A}})_\alpha] m_\alpha^{-1}}{\sum_\alpha |12V(\beta^2_G)_\alpha + 4V(\beta^2_{\mathcal{A}})_\alpha| m_\alpha^{-1}}, \quad (31)$$

where the summations are over all nuclei.

It has been shown that rotational ROA is small in comparison with vibrational ROA [40]. It will therefore make a negligible contribution only to the sum of absolute values that occur in the denominator of (31), where all terms are taken positive, and we can set

$$\sum_\alpha |12V(\beta^2_G)_\alpha + 4V(\beta^2_A)_\alpha| m_\alpha^{-1} \approx \sum_p^{\text{vib}} |12\beta^2_{Gp} + 4\beta^2_{\mathcal{A}p}|, \quad (32)$$

where the summation is over the vibrational modes of the molecule. In the numerator, we cannot neglect rotational contributions, however, because, in contrast to vibrational ROA, all rotational terms have the same sign [40]. Their fractional contribution in (31) can be formally written as

$$\delta(\text{rot}) = \frac{\sum_p^{\text{rot}} (12\beta^2_{Gp} + 4\beta^2_{\mathcal{A}p})}{\sum_p^{\text{vib}} |12\beta^2_{Gp} + 4\beta^2_{\mathcal{A}p}|} = \frac{\sum_\alpha [12V(\beta^2_G)_\alpha + 4V(\beta^2_{\mathcal{A}})_\alpha] m_\alpha^{-1} - \sum_p^{\text{vib}} (12\beta^2_{Gp} + 4\beta^2_{\mathcal{A}p})}{\sum_p^{\text{vib}} |12\beta^2_{Gp} + 4\beta^2_{\mathcal{A}p}|}. \quad (33)$$

Rotational ROA is determined by the anisotropy of purely electronic tensors. We can therefore consider it an expression of electronic chirality. Subtracting (33) from (31) then yields a measure of the influence of the chiral distribution of a molecule's electrons on vibrational ROA alone:

$$\delta(\text{vib}) = \frac{\sum_p^{\text{vib}} (12\beta^2_{Gp} + 4\beta^2_{\mathcal{A}p})}{\sum_p^{\text{vib}} |12\beta^2_{Gp} + 4\beta^2_{Ap}|}. \quad (34)$$

Analogous expressions pertain to other scattering geometries.

Comparison with the experiment can be made by multiplying the measured ROA difference intensities, expressed as the difference ΔN_p of scattered photons for right and left circularly polarized light by vibration p, multiplied by appropriate frequency and Boltzmann factors:

$$\delta(\text{vib}) = \frac{\sum_p \Delta N_p \Delta\omega_p [1 - \exp(-\hbar\Delta\omega_p/kT)]/\omega_p^3}{\sum_p |\Delta N_p| \Delta\omega_p [1 - \exp(-\hbar\Delta\omega_p/kT)]/\omega_p^3}. \quad (35)$$

In choosing the frequency factors in (35), it has been assumed that the spectral linewidth of individual vibrational bands is narrow enough so that they can be characterized by a single discrete vibrational frequency $\Delta\omega_p$.

For [$^2H_1$, $^2H_2$, $^2H_3$]-neopentane, $\delta(\text{vib}) = -\delta(\text{rot})$ as $\delta(\text{rovib})$ vanishes according to (29). According to [40], $\delta(\text{rot})$ is expected to vanish as electronic tensors for a T_d symmetric electron distribution have no anisotropic part. The calculated values of $\delta(\text{vib})$ are negligible, as expected, and the deviation from zero below the computational precision.

Of particular interest is the cumulative sum which one obtains by the stepwise adding of the VOA intensities of individual vibrations, starting with the vibration of the lowest and progressing to vibrations of higher energy. Normalized by the full denominator of Eq. (34), it is represented graphically for ROA and VCD in Figure 16. The value at the left-hand side of Figure 16 represents the value of $\delta(\text{vib})$, Eq. (34), i.e., the sum over all vibrations. The cumulative sum tends to return to a zero value after relatively small spectral sections, and in particular after the low frequency region of major VOA discussed earlier, as well as the CD- and the CH-stretch region.

The spectral ranges over which cancelation occurs are similar for ROA and VCD, and similar for all rotamers. Clearly, nuclear motion is strongly coupled within such regions of vibrational energy, but largely independent for the different regions. This brings to mind a venerable technique of the pre-computer age for simplifying otherwise untractable problems of a vibrational analysis, namely by the selection of spectral regions of interest through putting certain force constants in internal coordinates either to zero or to infinity [37].

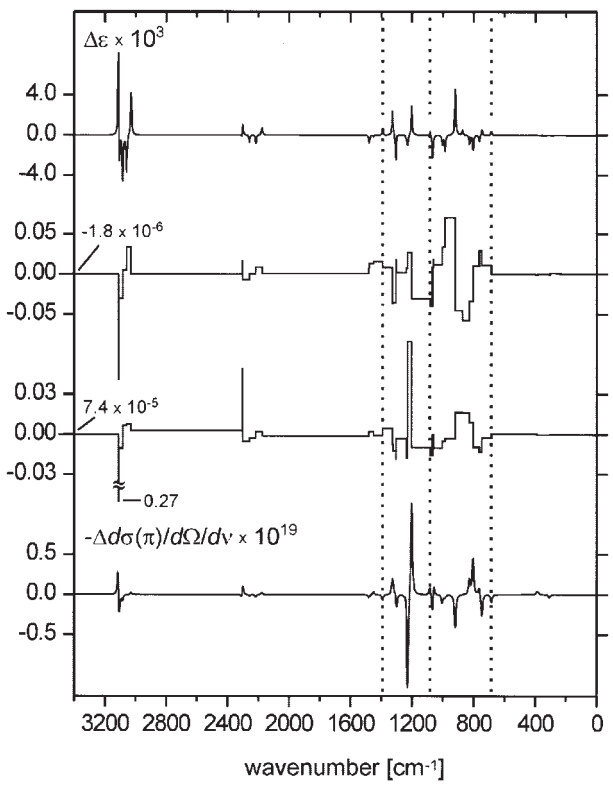

FIGURE 16. Cumulated normalized sums of the VCD (top half) and the ROA (bottom half) according to Eqs. (34) and (35), for rotamer 5 of (R)-[$^2H_1$, $^2H_2$, $^2H_3$]-neopentane. Summation starts with vibration 1 at the right-hand side. The value of the cumulated sum goes from positive to negative approximately between the two spectral regions of major VOA indicated in Figs. 8 and 9, and returns to zero between the lower-frequency region, the CD-stretch, and the CH-stretch region. Actual ROA and VCD spectra are included for comparison. Computational parameters: as in Fig. 2.

Conclusions

There can be little doubt that [$^2H_1$, $^2H_2$, $^2H_3$]-neopentane is one of the most spectacular, and perhaps indeed the most spectacular, chiral molecule in the field of vibrational optical activity. At the outset, it might look like a very special case, with little relevance to the molecules stereochemists encounter in their everyday work. Upon closer inspection, it becomes clear, however, that the molecule is a treasure trove for the separate study of many aspects of the generation of vibrational optical activity which are confounded in most chiral molecules.

One of these aspects we had not expected to encounter is the apparent importance of inertial contributions for the VOA of the CH- and CD-stretch vibrations. They lead to ROA and VCD of the same sign, despite the opposite sign convention of the two methods. Another unexpected result is the roughly mirror image appearance of VCD and ROA in the region of lower vibrational energies. Both findings are independent of the computational approach used and merit further investigation.

For the CH- and CD-stretch region, the similarity of ROA and VCD manifests itself for vibrations of individual rotamers, and the conclusion that inertial contributions are decisive is supported by the opposite signs which the CH- and CD-stretch vibrations produce for sister vibrations in rotamers which are related through the interchange of H and D nuclei. For the lower-energy region, the mirror image appearance of ROA and VCD is best visible for the mixture of the nine rotamers of the molecule, where it is clear cut. For vibrations of individual rotamers it can be absent, as Figure 15 demonstrates for the prominent vibrations 23 and 24 of rotamer 5.

A result that we expected, and looking for which provided the original incentive for our theoretical investigation of [$^2H_1$, $^2H_2$, $^2H_3$]-neopentane, is that the total ROA, summed for all vibrations according to Eqs. (34) and (35), is negligible. This is not only the case for the ROA of all vibrations, but to fair approximation also for individual spectral regions, namely the CH-stretch, the CD-stretch, and the lower-frequency region. The results are very similar for VCD. In view of Eq. (29), this makes it evident that the vibrational motions of these three energy regions are largely independent of each other. This is a result that we expect to hold approximately for most chiral molecules.

Another important goal of this study has been to computationally assess the measurability of the ROA and the VCD of the enantiomers of [$^2H_1$, $^2H_2$, $^2H_3$]-neopentane. If measurable, the molecule is of enough intellectual interest so that it will be synthesized by stereochemists. According to some inquiries we made to this end, the synthesis, while not trivial, appears feasible. We have therefore been as careful as possible in judging the measurability of the VOA of the compound, including the use of realistic band shapes of the Voigt type to simulate expected spectra. The ROA, while not generous for the mixture of rotamers due to canceling, should nevertheless be measurable in the 700–1,400-cm^{-1} region, with only a few milligrams of substance.

The g-values for VCD are far larger than the Δ-values for ROA, and VCD should therefore easily be measurable in the 700–1,100-cm^{-1} region and beyond, including with scanning instruments of low spectral resolution [30]. This prediction assumes that enough substance becomes available, as the vibrational absorption of the nonpolar compound with its T_d symmetric electron distribution is small.

The physical properties of [$^2H_1$, $^2H_2$, $^2H_3$]-neopentane are not expected to present an obstacle to a measurement. The boiling point of neopentane itself is 9.5°C, so it can be handled as a liquid under slight pressure or with refrigeration.

Some questions have only been touched upon, such as why the signs of the ROA and VCD of [$^2H_1$, $^2H_2$, $^2H_3$]-neopentane are related in such a peculiar way. Other aspects of the molecule's VOA, and of its vibrational spectrum in general, have not even been mentioned in this article, e.g., the relative sign pattern of quadrupole and magnetic dipole contributions. One aspect that needs closer scrutiny is the influence the many approximations that enter VCD and ROA calculations can have on numerical results. The methods we use are well tested, but [$^2H_1$, $^2H_2$, $^2H_3$]-neopentane is also a molecule particularly well suited to assess some of the limits of present VOA calculations. Questions of this kind remain the subject of future work. Nevertheless, we hope we have been able to show that modern ab initio computations, combined with innovative graphic methods, can make a decisive contribution to the understanding of vibrational spectra.

ACKNOWLEDGMENTS

Some of the pilot calculations of [$^2H_1$, $^2H_2$, $^2H_3$]-neopentane, and tests on the realistic representation of its spectra, were done by Mehdi Bounouar in the frame of his diploma work with one of the authors (W.H.). Some of the original MATLAB routines for visualising ACPs and GCMs were written by Gérard Zuber.

References

1. Hug, W. In Raman Spectroscopy, Linear and Nonlinear; Lascomb, J.; Huong, P., Eds.; Wiley-Heyden: Chichester, 1982; p 3.
2. (a) Barron, L. D. J Chem Soc Chem Commun 1977, 305; (b) Barron, L. D.; Numan, H.; Wynberg, H. J Chem Soc Chem Commun 1978, 259; (c) Holzwarth, G.; Hsu, E. C.; Mosher, H. S.; Faulkner, T. R.; Moscowitz, A. J Am Chem Soc 1974, 96, 251; (d) Stephens, P. J.; Clark, R. In Optical Activity and Chiral Discrimination; Mason, S. F., Ed.; D. Riedel: Dordrecht, 1979; (e) Polavarapu, P. L.; Nafie, L. A.; Benner, S. A.; Morton, T. H. J Am Chem Soc 1981, 103, 5349.
3. Hug, W. In Handbook of Vibrational Spectroscopy; Chalmers, J. M.; Griffiths, P. R., Eds.; John Wiley & Sons: Chichester, 2002; Vol 1, p 745.
4. Nafie, L. A. Chem Phys 1996, 205, 309.
5. Constante, J.; Hecht, L.; Polavarapu, P. L.; Collet, A.; Barron, L. D. Angew Chem Int Ed 1997, 36, 885.
6. Wynberg, H. Acc Chem Res 1971 4, 65.
7. Barron, L. D. Molecular Light Scattering and Optical Activity, 2nd ed.; Cambridge University Press: Cambridge, 2004.
8. Freedman, T. B.; Nafie, L. A. In Modern Nonlinear Optics; Evans, M.; Kielich, S., Eds.; Wiley: New York, 1994; Part 3, p 207.
9. Placzek, G. Handbuch der Radiologie; Marx, E., Ed.; Akademische Verlagsgesellschaft: Leipzig, 1934; Vol VI, p 205.
10. Barron, L. D.; Hecht, L.; Gargaro, A. R.; Hug, W. J Raman Spectrosc 1990, 21, 375.
11. (a) Barron, L. D.; Hecht, L.; Hug, W.; MacIntosh, M. J. J Am Chem Soc 1989, 111, 8731; (b) Hecht, L.; Barron, L. D.; Hug, W. Chem Phys Lett 1989, 158, 341.
12. Barron, L. D.; Buckingham, A. D. Mol Phys 1971, 20, 1111.
13. Long, D. A. Raman Spectroscopy; McGraw-Hill: New York, 1977; p 130.
14. (a) Nafie, L. A. J Chem Phys 1983, 79, 4950; (b) Nafie, L. A. J Chem Phys 1992, 96, 5687.
15. Hug, W. Chem Phys 2001, 264, 53.
16. Buckingham, A. D. Faraday Discuss 1994, 99, 1.
17. (a) Hug, W.; Surbeck, H. Chem Phys Lett 1979, 60, 186; (b) Barron, L. D. Chem Phys Lett 1983, 102, 285; (c) Nafie, L. A. Chem Phys Lett 1983, 102, 287.
18. (a) Devlin, F. J.; Stephens, P. J.; Cheeseman, J. R.; Frisch, M. J. J Phys Chem 1997, 101, 6322; (b) Devlin, F. J.; Stephens, P. J.; Cheeseman, J. R.; Frisch, M. J. J Phys Chem 1997, 101, 9912.
19. Cheeseman, J. R.; Frisch, M. J.; Devlin, F. J.; Stephens, P. J Chem Phys Lett 1996, 252, 211.
20. Frisch, M. J.; Trucks, G. W.; Schlegel, H. B.; Scuseria, G. E.; Robb, M. A.; Cheeseman, J. R.; Montgomery, J. A., Jr.; Vreven, T.; Kudin, K. N.; Burant, J. C.; Millam, J. M.; Iyengar, S. S.; Tomasi, J.; Barone, V.; Mennucci, B.; Cossi, M.; Scalmani, G.; Rega, N.; Petersson, G. A.; Nakatsuji, H.; Hada, M.; Ehara, M.; Toyota, K.; Fukuda, R.; Hasegawa, J.; Ishida, M.; Nakajima, T.; Honda, Y.; Kitao, O.; Nakai, H.; Klene, M.; Li, X.; Knox, J. E.; Hratchian, H. P.; Cross, J. B.; Bakken, V.; Adamo, C.; Jaramillo, J.; Gomperts, R.; Stratmann, R. E.; Yazyev, O.; Austin, A. J.; Cammi, R.; Pomelli, C.; Ochterski, J. W.; Ayala, P. Y.; Morokuma, K.; Voth, G. A.; Salvador, P.; Dannenberg, J. J.; Zakrzewski, V. G.; Dapprich, S.; Daniels, A. D.; Strain, M. C.; Farkas, O.; Malick, D. K.; Rabuck, A. D.; Raghavachari, K.; Foresman, J. B.; Ortiz, J. V.; Cui, Q.; Baboul, A. G.; Clifford, S.; Cioslowski, J.; Stefanov, B. B.; Liu, G.; Liashenko, A.; Piskorz, P.; Komaromi, I.; Martin, R. L.; Fox, D. J.; Keith, T.; Al-Laham, M. A.; Peng, C. Y.; Nanayakkara, A.; Challacombe, M.; Gill, P. M. W.; Johnson, B.; Chen, W.; Wong, M. W.; Gonzalez, C.; and Pople, J. A. Gaussian 03, Revision C.03; Gaussian: Wallingford, CT, 2004.
21. (a) Becke, A. D. J Chem Phys 1993, 98, 5648; (b) Lee, C.; Yang, W.; Parr, R. G. Phys Rev B 1988, 37, 785.

22. Krishnan, R.; Binkley, J. S.; Seeger, R.; Pople, J. A. J Chem Phys 1980, 72, 650.
23. Kendal, R. A.; Dunning, T. H.; Harrison, R. J. J Chem Phys 1992, 96, 6796.
24. (a) Oddershede, J.; Jørgensen, P.; Yeager, D. L. Comput Phys Rep 1984, 2, 33; (b) Jørgensen, P.; Jensen, H. J. Aa.; Olsen, J. J Chem Phys 1988, 89, 3654.
25. Helgaker, T.; Jensen, H. J. Aa.; Jørgensen, P.; Olsen, J.; Ruud, K.; Ågren, H.; Auer, A. A.; Bak, K. L.; Bakken, V.; Christiansen, O.; Coriani, S.; Dahle, P.; Dalskov, E. K.; Enevoldsen, T.; Fernandez, B.; Hättig, C.; Hald, K.; Halkier, A.; Heiberg, H.; Hettema, H.; Jonsson, D.; Kirpekar, S.; Kobayashi, R.; Koch, H.; Mikkelsen, K. V.; Norman, P.; Packer, M. J.; Pedersen, T. B.; Ruden, T. A.; Sanchez, A.; Saue, T.; Sauer, S. P. A.; Schimmelpfennig, B.; Sylvester-Hvid, K. O.; Taylor, P. R.; Vahtras, O. DALTON, A Molecular Electronic Structure Program, Release 1.1; 2000, see http://www.kjemi.uio.no/software/dalton/dalton.html.
26. MATLAB Version 6.1 Release 12.1; Mathworks: Natick, CA, 2001.
27. Berg, M.; Vanden Bout, D. A. Acc Chem Res 1997, 30, 65.
28. Hubble, H. W.; Lai, T.; Berg, M. A. J Chem Phys 2001, 114, 3662.
29. Hug, W.; Hangartner, G. J. Raman Spectrosc 1999, 30, 841.
30. Keiderling, T. A. In Biomolecular Structure and Dynamics; NATO ASI series, Series E: Applied Sciences; Vergoten, G.; Theophanides, T., Eds.; Kluwer Academic: Dordrecht, The Netherlands, 1997; Vol 342, p 299.
31. Herzberg, G. H. Molecular Spectra and Molecular Structure. II. Infrared and Raman Spectra of Polyatomic Molecules; Van Nostrand: Princeton, NJ, 1945.
32. Dollish, F. R.; Fateley, W. G. Characteristic Raman Frequencies of Organic Compounds; John Wiley & Sons: New York, 1974.
33. Colthup, N. B.; Daly, L. H.; Wiberley, S. E. Introduction to Infrared and Raman Spectroscopy; Academic Press: New York, 1975.
34. Zuber, G.; Hug, W. Helv Chim Acta 2004, 87, 2208.
35. (a) Nafie, L. A.; Yu, G.-S.; Qu, X.; Freedman, T. B. Faraday Discuss 1994, 99, 13; (b) Tam, C. N.; Bouř, P.; Keiderling, T. A. J Am Chem Soc 1997, 119, 7061.
36. Hug, W. Appl Spectrosc 2003, 57, 1.
37. Wilson, E. B.; Decius, J. C.; Cross, P. C. Molecular Vibrations; Dover: New York, 1955.
38. Kauzmann, W. Quantum Chemistry; Academic Press: New York, 1957; p 711.
39. Cuony, B.; Hug, W. Chem Phys Lett 1981, 84, 131.
40. Barron, L. D.; Johnston, C. J. J. Raman Spectrosc 1985, 16, 208.